A probabilistic method for the estimation of ocean surface currents from short time series of HF radar data

Charles-Antoine Guérin, Stéphan T. Grilli

A probabilistic method for the estimation of ocean surface currents from short time series of HF radar data

Charles-Antoine Guérin

Univ Toulon, Aix Marseille Univ, CNRS/INSU, IRD, MIO UM 110, Mediterranean Institute of Oceanography, La Garde, France

Stéphan T. Grilli

Department of Ocean Engineering, University of Rhode Island, Narragansett, RI, USA

Abstract

We present a new method for inverting ocean surface currents from beamforming HF radar data. In contrast with the classical method, which inverts radial currents based on shifts of the main Bragg line in the radar Doppler spectrum, the method works in the temporal domain and inverts currents from the amplitude modulation of the I and Q radar time series. Based on this principle, we propose a Maximum Likelihood approach, which can be combined with a Bayesian inference method assuming a prior current distribution, to infer values of the radial surface currents. We assess the method performance by using synthetic radar signal as well as field data, and systematically comparing results with those of the Doppler method. The new method is found advantageous for its robustness to noise at long range, its ability to accommodate shorter time series, and the possibility to use *a priori* information to improve the estimates. Limitations are related to current sign errors at far-ranges and biased estimates for small current values and very short samples. We apply the new technique to a data set from a typical 13.5 MHz WERA radar, acquired off of Vancouver Island, BC, and show that it can potentially improve standard synoptic current mapping.

Keywords: HR radar, ocean surface current, Bayesian estimation

1. Introduction

In the past four decades, High Frequency (HF) radars have routinely been used to monitor ocean surface currents in coastal regions (see, e.g., the reviews [1, 2]) and, more recently, to estimate other sea state parameters (see the recent review in [3, 4, 5]). HF radars take advantage of two specific physical mechanisms occurring in the HF electromagnetic (EM) wave regime, namely the over-the-horizon propagation of EM surface waves, for a vertically polarized electric field, and the dominance in the backscattered signal of a single resonant component of the ocean wave field, a process known as "Bragg scattering". The estimation of ocean surface currents along the radar looking direction (referred to as "radial surface currents") is typically based on identifying the frequency shift caused by the current in the backscattered Doppler spectrum to the well-defined Bragg frequency line. The performance of this estimation, in terms of accuracy, reliability, achievable range, and spatial resolution, depends on several parameters related to the radar system (e.g., carrier frequency, antenna system, integration time, emitted power), the environment (e.g., sea state, Radio Frequency Interferences ("RFI"), or a combination of both (signal-to-noise ratio ("SNR")).

Even though the physics underlying the estimation of ocean surface currents through Bragg scattering has been well understood for a long time, we show in this paper that the processing of the radar signal can still be improved. To this effect, we propose a new non-spectral estimator that can recover (or invert) radial currents from complex radar time series, based on a Maximum Likelihood Bayesian optimization approach. The main principle of the new estimator is that, in the HF regime, ocean surface currents cause a slow amplitude modulation of the real and imaginary parts of the backscattered radar signal which, depending on the level and nature of the environmental noise affecting the data, may in some cases be easier to identify than a shift in the main spectral peak in the Doppler spectrum. Additionally, the estimation based on the amplitude modulation can be improved by resorting to Bayesian inference,

in which an *a posteriori* probability distribution is derived for the estimated parameter (here the radial current), given the observations and some *a priori* information. The estimation then results from maximizing the likelihood of the *a posteriori* probability distribution (i.e., minimizing errors). The introduction of *a priori* information on radial surface currents reduces the undesirable occurrence of outliers and the dispersion of the estimates. As a result, with the new estimator, shorter time series of radar signal can in principle be used to achieve a specified confidence interval on the inverted currents, than with the Doppler-based estimation. These properties of the new estimator will be made clear in the paper.

In physical studies of ocean surface currents inverted from HF radar data based on the standard Doppler method, the time scales considered are typically on the order of 2 to 60 minutes, depending on radar frequency, the antenna system (compact antenna or large arrays), and signal-to-noise ratio. The selected observation time results from a trade-off between the conflicting requirements of using a large enough integration time to accurately compute the spectra and achieve sufficient resolution on the currents, and a short enough time to capture the temporal variability of mesoscale oceanic features. A number of studies of ocean surface currents at such spatial scales have shown that an integration/observation time on the order of 20 minutes is in general adequate to characterize most classical patterns of background oceanic currents, such as rapidly evolving eddies, tidal and subtidal fluctuations, and the ocean response to a changing wind stress (see references in [3, 4]). However, for some emerging applications, such as the early detection of tsunamis (e.g. [6, 7, 8]) and particularly the non-seismic tsunamis (e.g., meteotsunamis, landslide tsunamis), which have shorter wavelengths, a shorter integration time is required to properly capture the signature of such events in ocean surface currents, whose typical period is on the order of a few to a few tens of minutes [9]. Other applications such as the prediction of Lagrangian transport in oil spill tracking (e.g., [10]), the distribution of plankton blooms in ecological systems ([11]), or the identification of small-scale coherent structures (e.g. [12, 13]), while not restricted to,

would clearly benefit from a higher temporal resolution in the inverted surface currents. The reliable estimate of small magnitude surface currents varying at minute temporal scales would also make it possible observing infragravity waves, through the measurement of their orbital motion, which have a typical period of 30 sec to a few minutes ([14]). Such waves, which are generated and grow in parallel with large storm systems, are key contributors to the coastal flooding and erosion such storms cause upon landing.

Estimating the Bragg frequency shift in the time domain is not new, and several attempts have been made in the literature to carry it out using non-spectral parametric methods (see [29] for a comprehensive review). Kahn [30] studied the rapid variations (at the sub-minute time scale) of oceanic HF backscattered signal in the context of target detection and sea clutter suppression. He observed amplitude modulations of the HF radar time signal (his Figs. 2 and 3), which he attributed to velocity variations of ocean waves. He then proposed tracking short term variations of the main frequency around the Bragg line via an autoregressive, low-order linear, prediction model, which he showed predicted well the observed modulations of the radar signal. This made it possible demodulating the radar signal and discriminating the target, by filtering out the rapid variations of the Bragg peak. An interesting application of this for surface current estimation at a rapid time scale is the interpretation of the shifted Bragg frequency in terms of the complex roots of the prediction-error filter on the unit circle. The idea of using an autoregressive approach in the time domain for improving the estimation of surface currents was later applied by [31]. An instantaneous Bragg frequency, calculated on short samples (256 points), was obtained through the coefficient of the autoregressive model and the resulting estimated current was shown to be more realistic, in the sense that it did not suffer from rapid non-physical fluctuations in time, such as observed with the Doppler approach. This technique has no physical basis or constraint other than that the difference between the positive and negative Bragg peak frequencies must be twice the Bragg frequency. Another method dealing with instantaneous variations in the Bragg peak frequency was the Instantaneous-

Filtering technique proposed by [32], who used it to identify and remove the frequency modulation due to the ocean variability. Our probabilistic approach belongs to the same family of parametric non-spectral techniques, as it accurately estimates instantaneous frequencies. Its main difference in purpose with these earlier approaches, however, is that it is not based on a filtering techniques but instead constrains the signal to match a physical (albeit simplistic) analytical model, namely the first-order Bragg theory, while other methods proposed earlier were entirely empirical. Another important feature of the new method is the possibility to incorporate *a priori* information in the current estimation. We did not yet perform a systematic comparison of our method with the earlier alternative methods for estimating radial surface currents; this task will be left out for future work.

In this paper, in Section 2, we first review the classical spectral estimation method and summarize its main features and limitations. In Section 3 we introduce a key simplified representation of the radar signal, within the frame of first-order Bragg theory, which in Section 4 naturally leads to the formulation of the new estimator of radial surface currents. The general performance of the estimator is then assessed in Sections 5 and 6, first on the basis of synthetic radar data. In Section 7, the new method is finally applied to an actual data set of HF data, recently acquired by a WERA radar system installed in Tofino (BC, Canada) to monitor ocean surface currents off of Vancouver Island. Based on a few test cases, we show that the new method has the potential of both better capturing the variability of surface currents at short time scales and extending the spatial coverage of standard synoptic current mapping. A critical discussion of the method is provided in Section 8, where its potential limitations and improvements are presented.

2. A review of the classical estimation method

Crombie [15] first identified the main principle underlying the estimation of ocean surface currents on the basis of HF radar data and, subsequently, Barrick

[16, 17, 18, 19] provided its theoretical foundation. The latter relies on Rayleigh-Rice's perturbation theory for a scattered electromagnetic field, which is valid when the vertical scale of elevation is much smaller than the radar wavelength. In the context of ocean remote sensing, this theory is commonly referred to as "Bragg scattering", due to its formal similarity with the diffraction mechanism occurring in crystalline solids.

To the first-order in ocean wave steepness, the dominant contribution to the backscattered radar field is associated with an ocean wave of specific wavelength, of vector wavenumber $\boldsymbol{K}_B$, referred to as the "Bragg wave". This wave is defined by the resonant condition $\boldsymbol{K}_B = -2\boldsymbol{K}_0$, where $\boldsymbol{K}_0$ is the horizontal projection of the EM wave vector. At grazing incidence, the Bragg wave has half the radar EM wavelength and propagates in either direction along the radar looking direction. The resulting backscattered temporal echo (i.e., the radar signal) is affected by a Doppler frequency shift proportional to the celerity of the Bragg wave. Assuming purely gravity waves in deep water, the resonant condition yields the well-known expression of the Bragg (circular) frequency,

$$\omega_B = 2\pi\sqrt{\frac{gf_0}{\pi c_0}} \tag{2.1}$$

in which f_0 denotes the radar frequency and c_0 is the celerity of light in a vaccum.

On this basis, the so-called backscattered Doppler spectrum $\sigma(\omega)$ is defined as the average normalized radar cross-section per unit bandwidth. Within the framework of first-order Bragg theory applied to a random sea surface, in the absence of a current, Barrick [16, 17, 18, 19] derived its expression as,

$$\sigma(\omega) = 2^6\pi K_0^4\Big\{ S_d(+\boldsymbol{K}_B)\,\delta(\omega-\omega_B) + S_d(-\boldsymbol{K}_B)\,\delta(\omega+\omega_B)\Big\}, \tag{2.2}$$

where S_d is the directional (non-symmetrical) wave energy density spectrum and the Dirac δ functions represent two spectral lines at plus or minus the Bragg frequency.

In the presence of a stationary surface current of velocity $\boldsymbol{U}$, the two Bragg lines are translated in frequency by a value ω_c, resulting from the additional

Doppler shift caused by the current advection in the radar looking direction. Discarding the sign at this stage this is defined by,

$$\omega_c = \frac{4\pi\,|U_r|}{\lambda_o}, \tag{2.3}$$

where $U_r = \boldsymbol{U}\cdot\boldsymbol{R}$ is the radial surface current, that is the component of the current along the radar looking direction, and λ_o the radar wavelength. As was shown in [20], this result is exact to the first-order in wave steepness when U_r is the vertically-averaged current over a surface layer of thickness $\lambda_o/(2\pi)$. The first-order Doppler spectrum in the presence of a current therefore reads,

$$\sigma(\omega) = 2^6\pi K_0^4\Big\{S_d(+\boldsymbol{K}_B)\delta(\omega-\omega_B+\epsilon_c\omega_c)+S_d(-\boldsymbol{K}_B)\delta(\omega+\omega_B+\epsilon_c\omega_c)\Big\}, \tag{2.4}$$

where $\epsilon_c = \pm 1$ is the sign of the additional Doppler shift induced by the current, depending on whether it is flowing towards ($\epsilon_c = +1$) or away ($\epsilon_c = -1$) from the radar. Measuring the frequency shift ω_c, between the actual and theoretical values of the Bragg lines in the radar Doppler spectrum, allows inverting for the algebraic value of the radial current U_r, using Eq.(2.3).

As this is well-known and not the object of this paper, we will not belabor here the main steps of radar signal processing, which make it possible to transform the backscattered electromagnetic field on the antenna system into a complex electric signal resolved, in both range (R) and azimuth (Φ), over a grid of "radar cells" defined on the sea surface. We will refer to, e.g., [21] for a review of the main techniques underlying the operational use of HF radars and their features and limitations.

In the following, $s(t)$ refers to the complex time series of processed backscattered radar signal measured in a given radar cell, located at a specific range R and azimuth Φ. Within a calibration factor, the Doppler spectrum of this signal is given by,

$$\sigma(\omega) = \lim_{T\to+\infty}\frac{1}{T}\langle\left|\int_{-T/2}^{+T/2} e^{\mathrm{i}\omega\mathrm{t}}s(t)\,\mathrm{d}t\right|^2\rangle, \tag{2.5}$$

where $\langle\cdot\rangle$ denotes an ensemble average, which can be computed as the mean over successive incoherent samples. The Doppler spectrum is easily calculated via

a Fast Fourier Transform, which can be applied to the measured backscattered signal either before or after it has been processed in azimuth by a beam-forming. In the classical technique of estimating radial currents based on measuring the shift of the main Bragg lines, according to Eq. (2.4), the order in which these operations are performed is not important. However, for the new method proposed here, which is based on time series of range-azimuth resolved radar signal, it is necessary that the azimuthal processing occur first, that is before any Doppler processing. Note that this implies that the new method cannot be applied to data from compact radar systems, where the azimuthal resolution is achieved in the frequency domain, and its applicability is thus limited to radar systems using beam-forming techniques.

Defining the accuracy of the radial current estimates is a delicate matter, which requires both physical and radar processing considerations. This accuracy is usually related to the width of the Bragg peak, which is controlled by two main phenomena. The first one is the broadening of the main Bragg line du to signal modulations by long waves, resulting from induced orbital currents. The second one is the effect of the finite integration time T used in Eq. (2.5), which results in a frequency resolution $\Delta\omega \sim 2\pi/T$ and a broadening by the same amount of the theoretical Dirac δ function for the Bragg spectral line. For short integration times, the second phenomenon, that is the finite frequency resolution, is the main limiting factor, yielding a principal resolution of the estimated radial currents of $\Delta U_r = \lambda_o/2T$. In fact, when estimating the Bragg peak frequency by the centroïd method (i.e., taking the barycenter of the Doppler spectrum over a few points surrounding the maximal spectral line), one can achieve a somewhat better accuracy than the FFT frequency resolution. As was shown in [22] (see Eqs. (21-23) and the corresponding discussion), the rms error on the peak frequency is the result of a compromise between the frequency resolution $\Delta\omega$, the number of spectral lines within the half-power peak, and the number of incoherent samples used to form the Doppler spectrum. Another important factor impacting the accuracy of current estimates is the noise level [23]. In operational conditions, the observation time required to achieve the afore-

mentioned accuracy can be larger in order to produce a sufficient SNR (i.e., the ratio of the main Bragg line peak power to the mean background power). However, the sample size cannot be taken arbitrary large as one must ensure stationarity of the sea state within the integration time (otherwise the accuracy could be reduced, e.g., by tidal variability). The choice of the observation time, hence, results from a compromise made between several conflicting requirements and corresponding parameters: update rate of the current estimation, effective accuracy, stationarity of sea state, and noise level.

Commercial software available in modern radar systems, such as WERA's, use complex and highly optimized algorithms to resolve the backscattered signal as a function of range and azimuth, which eliminate RFIs, select the Bragg lines of the radar data, and apply variance reduction techniques to the Doppler spectrum calculation [24, 25, 26, 27, 28]. Such optimizations are specific to the implemented algorithms and, hence, it would be difficult to make a general comparison between the performance of the new proposed method and the best available operational surface current measurement systems based on a spectral approach. Therefore, in the context of this study, we will only perform a theoretical comparison between the two signal processing methods using, for the spectral approach, a basic, non-optimized, algorithm, referred to as the "Doppler Method" (DM). In the DM, only the Bragg peaks in the radar spectrum that are larger than some threshold SNR are retained for the estimation of the current-induced Doppler shift, ω_c. In addition, an independently estimated maximum value of the radial current that can be reasonably expected to occur at the considered site is used to restrict the search domain for the shifted Bragg lines. These two conditions reduce the number of faulty estimates of the radial current, but usually yield incomplete current maps, having lacunary data at the most distant ranges. In the quantitative applications presented throughout this paper, the maximum current was set to 80 cm/s, unless stated otherwise; and the radial current magnitude was estimated from the mean position of the positive and negative maximal spectral lines (defined from a 3-point barycenter calculation around the maximal peak), whenever the two peaks have a SNR > 3

dB, or the most energetic peak otherwise.

3. Approximate expression of the complex radar signal

Applying first-order Bragg theory to the backscattered signal amplitude, rather than to its Doppler spectrum, the complex radar signal can be approximated in each radar cell by,

$$s(t) = A^{-}\mathrm{e}^{-\mathrm{i}(\omega_B - \epsilon_c\omega_c)t}\mathrm{e}^{-\mathrm{i}\varphi^{-}} + A^{+}\mathrm{e}^{+\mathrm{i}(\omega_B + \epsilon_c\omega_c)t}\mathrm{e}^{-\mathrm{i}\varphi^{+}}, \tag{3.6}$$

for some positive coefficients $A^{\pm}$ and random phase shifts $\varphi^{\pm}$, with,

$$s(t) = s_1(t) + \mathrm{i}\, s_2(t), \tag{3.7}$$

where s_1 and s_2 denote the real and imaginary parts of the complex radar signal, originating from the "I" and "Q" channels of the receiver.

Note that, in the following analysis, it will not be necessary to know the detailed expressions of coefficients $A^{\pm}$, in terms of sea state, radar system, and coordinates of the considered radar cells, but instead only their ratio, A^{+}/A^{-}. It should be pointed out that the model (3.6), selected to represent the backscattered time series of radar signal, is highly idealized as it ignores some physical effects, such as second-order components in Bragg theory, and the variability of the surface current within each grid cell (which may become important at far-ranges, where the azimuthal extent of radar cells is larger). However, we will show in the following that this simplified model is sufficient to achieve a good estimation of radial surface currents and, in Section 8, we provide some justifications for why these effects can be ignored.

We first illustrate the principle of the new current estimation method in a simple way, by considering the particular case of, $\epsilon_c = 1$, $A^{+} = A^{-} = A$, and $\varphi^{+} = \varphi^{-} = \varphi$, which for instance occurs when the two Bragg lines are of equal magnitude, yielding,

$$\begin{aligned} s_1(t) &= 2A\cos(\omega_c t - \varphi)\cos(\omega_B t) \\ s_2(t) &= 2A\sin(\omega_c t - \varphi)\cos(\omega_B t), \end{aligned} \tag{3.8}$$

which represents periodic oscillations of the radar signal components at the known Bragg frequency, modulated in amplitude by another oscillation caused by the unknown Doppler frequency shift ω_c. The principle of the new current estimation method is that the Doppler shift ω_c can be inferred from this amplitude modulation, from which the radial current $|U_r|$ can then be calculated with Eq. (2.3) without having to compute the radar Doppler spectrum. Hence, while the classical estimation of radial currents based on the Doppler spectrum takes place in the frequency space, requiring a spectral analysis, the new estimator proposed here detects the amplitude modulation of the radar signal directly in the time domain. Key advantages of this approach, as we shall see, are a shorter integration time than required to compute a meaningful Doppler spectrum and a greater robustness of the results (i.e., the inverted currents) to noise.

Next, Eq. (3.8) is generalized, albeit in an approximate manner, to the case of arbitrary amplitudes $A^{\pm}$ and phases $\varphi^{\pm}$. As detailed in Appendix, whenever $\omega_c \ll \omega_B$, the following are good approximations of s_1 and s_2 in the general case,

$$\begin{aligned} s_1(t) &\simeq \tilde{s}_1(t) = \alpha \cos(\omega_B(t-t_1)) \cos(\omega_c(t-t_1)) \\ s_2(t) &\simeq \tilde{s}_2(t) = \alpha \cos(\omega_B(t-t_2)) \cos(\omega_c(t-t_2)) \end{aligned} \tag{3.9}$$

where the reference times (t_1, t_2) and the amplitude α are defined as,

$$\begin{aligned} &t_1 = t(s_1^{max}),\ t_2 = t(s_2^{max}), \text{and} \\ &\alpha = \max(s_1, s_2), \ \text{ with } \ s_1^{max} = \max(s_1); s_2^{max} = \max(s_2) \end{aligned} \tag{3.10}$$

i.e., the time and magnitude of the maxima of s_1 and s_2, respectively.

Eqs. (3.9) for the I and Q signals can be used to estimate the Doppler shift ω_c and, in turn, the absolute value of the radial surface current, through the estimation of the amplitude α of an observed time series of complex backscattered signal $s(t)$, by way of a Least Square Method (LSM); importantly, this estimation does not require *a priori* knowledge of any other parameter, since the reference phases $(\omega_c t_1, \omega_c t_2)$ and α all follow from Eq. (3.10).

We define the normalized discrepancy D between the actual signal s from

Eq. (3.6) and its approximation $\tilde{s} = \tilde{s}_1 + \mathrm{i}\,\tilde{s}_2$ from Eq. (3.9) as,

$$D(s) = \frac{\|\mathbf{s} - \tilde{\mathbf{s}}\|^2}{\|\mathbf{s}\|^2} \quad \text{, with} \quad \|\mathbf{s}\|^2 = \frac{1}{T}\int_0^T |s(t)|^2 \, \mathrm{d}t, \tag{3.11}$$

the mean square norm of the radar signal over an integration time T. With this normalization, D only depends on the ratio of amplitudes of the positive and negative Bragg lines, i.e., parameter,

$$\rho = \frac{\min(A^-, A^+)}{\max(A^-, A^+)} \tag{3.12}$$

and the relative phase shift,

$$\varphi = \varphi^+ - \varphi^- \tag{3.13}$$

For given integration time T and Doppler frequency shift ω_c, D can be evaluated in a systematic manner by inspecting the complete (ρ, φ) domain. One can numerically show that the quality of the approximation is excellent when the respective amplitudes of the positive and negative frequencies are close to each other ($\rho \simeq 1$) regardless of their relative phase φ, but deteriorates as the amplitude ratio becomes smaller. This is consistent with the fact that an amplitude modulation can only be generated by the interference of two opposite frequencies.

In the presence of environmental noise, the evaluation of the amplitude parameter α with Eq. (3.10), through the maximum of the signal, becomes less accurate as noise can cause arbitrary high spurious values in the radar signal. In this case it becomes advantageous to rely on a time average over T, provided $T \gg T_c = 2\pi/\omega_c$. Indeed, since ω_B and ω_c have very different orders of magnitude, their time-average (i.e., mean square norm) is simply,

$$\frac{1}{T}\int_0^T \cos^2(\omega_B t)\cos^2(\omega_c t)\mathrm{d}t \simeq \frac{1}{4}, \tag{3.14}$$

yielding,

$$\alpha \simeq \sqrt{2}\,\|\mathbf{s}\|\,. \tag{3.15}$$

Fig. 1 shows an example of fitting the approximate Eq. (3.9) to idealized I and Q signals (Eq. 3.6), for 256 point samples ($T = 66$ s), in the presence of a

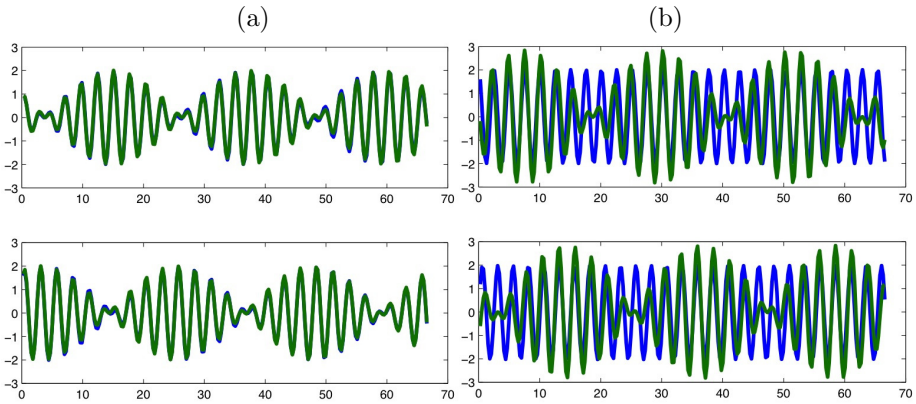

Figure 1: Time series of I and Q radar signals over a $T = 66$ s duration sample, for $U = 0.25$ cm/s, $\varphi = 2\pi/3$, and: (a) $A^{\pm} = 1$ ($\rho = 1$); (b) $A^{+} = 2, A^{-} = 0$ ($\rho = 0$). The blue curves are the actual signal form first-order Bragg formula (Eq. 3.6) and the green curves its approximation (Eq. (3.9))

$U_r = 0.25$ cm/s current, for a relative phase shift $\varphi = 2\pi/3$ and two extreme values of the amplitude ratio: $\rho = 1$ (optimal case), and $\rho = 0$ (unfavorable case), in Figs. 1a,b, respectively. The optimal value of ω_c is found by applying a standard LSM to the joint signals (s_1, s_2). The figures show, as expected, a perfect reconstruction in the first case but, even in the second case where there is no amplitude modulation, the model still captures well some of the main signal oscillations,which occur at the combined frequency $\omega_B + \omega_c$. This is made possible by the joint use of the I and Q signals, which imposes additional constraints on the relative phases and therefore on the value of ω_c.

The sign ϵ_c of the Doppler shift and, hence, the radial current direction (towards or away from the radar) can also be recovered by combining the signal's real and imaginary part estimates. Rewriting the approximation $\tilde{s} = \tilde{s}_1 + \mathrm{i}\,\tilde{s}_2$ in terms of complex exponentials and comparing with the initial expression of s in Eq. (3.6), we obtain a set of consistency relationships. Thus, for a positive Doppler shift ($\epsilon_c = +1$), the complex function $\tilde{s}$ should not contain any factor

$\mathrm{e}^{-\mathrm{i}\omega_c t}$, which implies,

$$\begin{aligned} C_A &= A^- \mathrm{e}^{-\mathrm{i}(\omega_B-\omega_c)t_1} + \mathrm{i}A^+ \mathrm{e}^{-\mathrm{i}(\omega_B-\omega_c)t_2} = 0 \\ C_B &= A^- \mathrm{e}^{\mathrm{i}(\omega_B+\omega_c)t_1} + \mathrm{i}A^+ \mathrm{e}^{\mathrm{i}(\omega_B+\omega_c)t_2} = 0 \end{aligned} \tag{3.16}$$

Likewise, for a negative Doppler shift ($\epsilon_c = -1$), $\tilde{s}$ should not contain any factor $\mathrm{e}^{+\mathrm{i}\omega_c t}$, that is,

$$\begin{aligned} C_C &= A^- \mathrm{e}^{-\mathrm{i}(\omega_B+\omega_c)t_1} + \mathrm{i}A^+ \mathrm{e}^{-\mathrm{i}(\omega_B+\omega_c)t_2} = 0 \\ C_D &= A^- \mathrm{e}^{\mathrm{i}(\omega_B-\omega_c)t_1} + \mathrm{i}A^+ \mathrm{e}^{\mathrm{i}(\omega_B-\omega_c)t_2} = 0 \end{aligned} \tag{3.17}$$

Hence, an estimator of the Doppler shift sign is obtained as,

$$\epsilon_c = \mathrm{sign}(|C_D\, C_C| - |C_A\, C_B|) \tag{3.18}$$

which can also be calculated based on radar signal data (see below for examples).

4. New estimators for the radial surface current

A new estimator of the radial current U_r can now be defined based on Eq. (3.9). Assuming the radar signal $s(t)$ is measured at N times $t_n = n\,\Delta t$ ($n = 1, ..., N$), i.e., $s_n = s(t_n)$, and representing it by Eq. (3.6) with the addition of a complex Gaussian noise of standard deviation σ_N, we have,

$$s_n = A^- \mathrm{e}^{-\mathrm{i}(\omega_B-\omega_c)t_n} \mathrm{e}^{-\mathrm{i}\varphi^-} + A^+ \mathrm{e}^{+\mathrm{i}(\omega_B+\omega_c)t_n} \mathrm{e}^{-\mathrm{i}\varphi^+} + \sigma_{\mathcal{N}}(X_n + iY_n), \tag{4.19}$$

where $X_n = \mathcal{N}(0,1)$ and $Y_n = \mathcal{N}(0,1)$ are normal random variables with zero mean and unit standard deviation. We denote by $s_{1,n}$ and $s_{2,n}$ (for $n = 1, ..., N$) the associated discrete time series of the signal real and imaginary parts, which will be separately analyzed. To devise an estimator that is independent of any calibration factor, we first recenter and renormalize these time series in such a way that (in view of Eq. (3.15)),

$$\frac{1}{N}\sum_{n=1}^{N} s_{1,n} = \frac{1}{N}\sum_{n=1}^{N} s_{2,n} = 0 \tag{4.20}$$

and,

$$\frac{1}{N}\sum_{n=1}^{N} s_{1,n}^2 = \frac{1}{N}\sum_{n=1}^{N} s_{2,n}^2 = \frac{1}{4} \tag{4.21}$$

Next, we use the approximate Eq. (3.9), which we assume to be exact, and rewrite,

$$\begin{aligned} s_{1,n} &= \tilde{s}_1(t_n;\omega_c) + \sigma_{\mathcal{N}} X_n \\ s_{2,n} &= \tilde{s}_2(t_n;\omega_c) + \sigma_{\mathcal{N}} Y_n \end{aligned} \tag{4.22}$$

with,

$$\begin{aligned} \tilde{s}_1(t_n;\omega_c) &= \cos(\omega_B(t_n - t_1))\cos(\omega_c(t_n - t_1)) \\ \tilde{s}_2(t_n;\omega_c) &= \cos(\omega_B(t_n - t_2))\cos(\omega_c(t_n - t_2)), \end{aligned} \tag{4.23}$$

and $t_1 = t(s_1^{max}),\ t_2 = t(s_2^{max})$.

According to this model, the Likelihood $\mathcal{L}(U_r|s_n)$ of the absolute radial current, $U_r = \lambda_o\omega_c/2$, given the observations s_n is given by,

$$\mathcal{L}(U_r|s_n) = \frac{1}{(2\pi\sigma_{\mathcal{N}}^2)^N} \exp\left(-\frac{D(U_r)}{2\sigma_{\mathcal{N}}^2}\right) \tag{4.24}$$

where,

$$D(U_r) = \sum_{n=1}^{N} \left\{ \tilde{s}_1(t_n;\omega) - s_{1,n} \right\}^2 + \sum_{n=1}^{N} \left\{ \tilde{s}_2(t_n;\omega) - s_{2,n} \right\}^2 \tag{4.25}$$

is the discrepancy, defined by Eq. (3.11), of the radar signal with respect to its approximation, expressed by Eq. (4.23) in the discrete case, for a trial radial current U_r. This leads to the classical Maximum (log) Likelihood Estimate (MLE) for the absolute radial current,

$$\widehat{U_r} = \arg\max\left(\log\mathcal{L}(U_r|s_n)\right) = \arg\min D(s_n;U_r) \tag{4.26}$$

In case of a weak SNR (or, equivalently, large $\sigma_{\mathcal{N}}$), the MLE can lead to non-physical estimates of the radial current, due to the occurrence of spurious maxima in the Likelihood function. This issue can partly be overcome by introducing *a priori* information on the distribution of radial currents and resorting to a Bayesian analysis. In this case, the *a posteriori* probability P of radial current, given the observations (which we simply denote by s_n, which should be understood as a generic term), is defined by,

$$P(U_r|s_n) = \mathcal{L}(U_r|s_n)\, P_0(U_r), \tag{4.27}$$

where P_0 is the prior distribution, that is the *a priori* probability distribution of the radial currents U_r in the absence of present observations. The knowledge of the prior distribution may result from reasonable physical assumptions or from prior measurements made over a long integration time. For instance, if a reasonable estimate of the mean radial current $\overline{U_r}$ is known, together with the maximum departure from this value, $2\sigma_{U_r}$, we may assume a normal prior distribution,

$$P_0(U_r) = \frac{1}{\sqrt{2\pi\sigma_{U_r}^2}} \exp\left(- \frac{(U_r - \overline{U_r})^2}{2\sigma_{U_r}^2} \right), \tag{4.28}$$

In this case, the absolute radial current U_r can again be estimated as the most probable value,

$$\widehat{U}_r = \arg\max\left(\log P(U_r|s_n)\right) = \arg\min\left(\frac{D(s_n;U_r)}{2\sigma_{\mathcal{N}}^2} + \frac{(U_r - \overline{U_r})^2}{2\sigma_{U_r}^2} \right) \tag{4.29}$$

Following the standard terminology we will henceforth refer to Eq. (4.29) as the "Maximum A Posteriori Probability Estimate" (MAPPE). In the absence of any *a priori* information (other than the maximum physical value U_r^{max}), the prior distribution is assumed uniform and the MAPPE coincides with the MLE, given by Eq. (4.26) on the selected search interval.

One difficulty of the Bayesian approach is that it requires knowledge of the noise level standard deviation $\sigma_{\mathcal{N}}$, which is a key parameter of the *a posteriori* distribution. However, a good estimate of the noise level can be obtained by differentiating the signal, which has the effect of damping its continuous deterministic part and enhancing its white noise components. Defining the sequences $\Delta s_{1,n} = s_{1,n+1} - s_{1,n}$ and $\Delta s_{2,n} = s_{2,n+1} - s_{2,n}$, we have from Eqs. (4.22) and (4.23):

$$\langle(\Delta s_{1,n})^2\rangle = \langle(\Delta s_{2,n})^2\rangle = \frac{1}{4}(\omega_B^2 + \omega_c^2)\Delta t^2 + 2\sigma_{\mathcal{N}}^2 \tag{4.30}$$

For a small sampling rate ($\sqrt{\omega_B^2 + \omega_c^2}\Delta t < 1$ and a small SNR ($\sigma_{\mathcal{N}} > 1$), this yields the estimate:

$$\sigma_{\mathcal{N}}^2 = \frac{1}{4}\langle(\Delta s_{1,n})^2 + (\Delta s_{2,n})^2\rangle \tag{4.31}$$

Note that the devised MLE and MAPPE estimators from Eqs. (4.26) and (4.29), only predict the absolute value of the radial current and not its sign.

Hence, once an estimate of the former has been obtained, the corresponding sign is inferred from Eq. (3.18). This will be made clearer in applications.

5. Performance assessment of the MLE

In the following, we assess the performance of the MLE estimator with respect to the DM. We do this in a simplified manner since, as pointed out before, it is difficult to make a general comparison between these methods as this depends on many parameters, such as radial current magnitude U_r, integration time T, noise level σ_N, and amplitude ratio ρ. Thus, we only perform basic tests of the estimator, to verify that it satisfies some minimal requirements. Here, we do not consider the performance of MAPPE, as it very much depends on the choice of the prior distribution.

We first investigated the MLE defined by Eq. (4.26) in the absence of noise ($\sigma_{\mathcal{N}} = 0$), using a large number $N = 128$ to 512 of (measured) signal realizations defined by Eq. (4.19), and sweeping a wide range of radial current magnitude U_r, with random phases $\varphi^{\pm}$ and various amplitude ratios ρ. Using the characteristics of the Tofino WERA HF radar, we performed Monte Carlo (MC) simulations to systematically investigate the current estimate bias, $\Delta U_r = \langle \widehat{U}_r \rangle - U_r$, for time series of duration $T =$ (i) 33 s (128 points); (ii) 66 s (256 points); and (iii) 133 s (512 points). This bias was found to have little dependence on the value of ρ, to be approximatively linear for small currents,

$$\Delta U_r \simeq \alpha(U_{r0} - U_r),\ U_r \leq U_{r0}, \tag{5.32}$$

and nearly zero for large currents, $\Delta U_r \simeq 0,\ U_r \geq U_{r0}$, where U_{r0} is some threshold, which is function of T. When U_r, U_{r0}, and ΔU_r are all expressed in cm/s, we found: (i) $T = 33$ s, $U_{r0} = 20,\ \alpha = 0.23$; (ii) $T = 66$ s, $U_{r0} = 13,\ \alpha = 0.55$; and (iii) $T = 133$ s, $U_{r0} = 5,\ \alpha = 2.5$.

Next, we systematically evaluated the MLE performance for different levels of noise $\sigma_{\mathcal{N}}$, and the mean and standard deviation of the estimated current were calculated for each actual value of the current. Fig. 2 shows results of such

estimations, made using $T = 33$ s samples (128 points), of a $U_r = 30$ cm/s radial current in a reasearch interval $[0 - 100]$ cm/s, for 3 representative values of the amplitude ratio $\rho = 0.1, 0.5$ and 1, and a noise level $\sigma_N = 0$ to 3.5, compared to similar estimations made using the DM. Results show that the DM performance strongly depends on the amplitude ratio and drastically deteriorates for small values of the latter. The MLE, however, only weakly depends on the amplitude ratio and shows a comparable performance to the DM otherwise. Even though the MLE is less accurate than the DM in the optimal case ($\rho = 1$), it is in general much more reliable when the level of noise increases. Based on the same analysis including noise, for other cases not shown here, we also found that the MLE remains an unbiased estimator ($\Delta U_r = \langle \widehat{U}_r \rangle - U_r \simeq 0$) except when both the current magnitude and the sample size N are small.

The quality of the estimation can be greatly improved when using *a priori* information, such as the probability distribution function of surface currents (prior distribution), as is done using MAPPE. This prevents the occurrence of outliers and considerably reduces the dispersion of estimated values. However, this can also introduce a bias if the prior distribution is centered about an erroneous value. Therefore, the use of *a priori* information must be made with caution and rests on the availability of reliable observations (such as the mean current estimated in the recent past).

6. Application of the MLE to synthetic HF radar data

6.1. Rapidly changing current

In this first application of the new MLE current estimator, we investigate its ability to estimate variations of the radial surface current occurring over short time scale (minutes), such as those induced by the propagation of very long waves, like infragravity waves or tsunamis. To this aim, we consider a current defined as a sinusoidal perturbation on top of a constant background current,

$$U_r(t) = 0.2 + 0.03 \cos\left\{2\pi \frac{t}{600}\right\} \qquad \text{(m/s)} \tag{6.33}$$

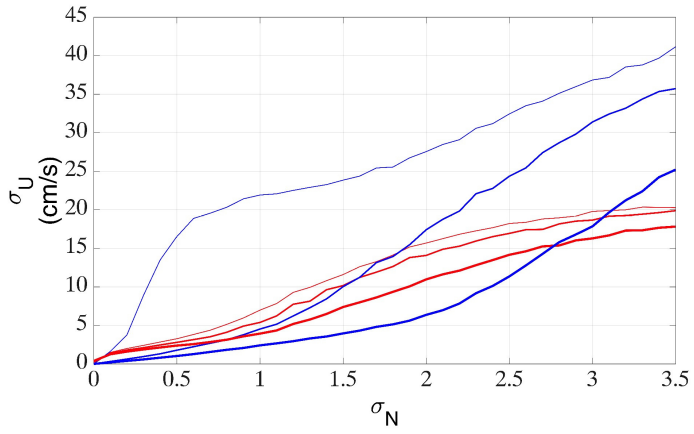

Figure 2: Standard deviation of radial surface current estimates using HF radar synthetic data ($T = 33$ s; $N = 128$), based on the MLE (red lines) or the DM (blue lines), as a function of noise level σ_N. The value of the radial surface current is $U_r = 30$ cm/s and, in the MLE, the current is searched within a 0 to 100 cm/s interval; three values of ρ are considered: $\rho = 0.1$ (thin lines), $\rho = 0.5$ (medium thick lines) and $\rho = 1$ (thick lines).

with a period of 600 s, which is typical of infragravity waves or landslide tsunamis [9]. We simulate the effect of this analytical current onto a synthetic radar time series generated with the noisy first-order Bragg model of Eq. (4.19), with $A^+ = 1$ and $A^- = 0.25$. Specifically, following the standard approach (e.g., [9]), the Doppler shift caused by this time varying current on the gravity wave dispersion relationship is simulated by replacing the phase $\omega_c\, t$ in Eq. (4.19) by a current "memory term" taking the form of an integral, i.e.,

$$\mathrm{e}^{i\epsilon_c \omega_c t} \rightarrow \mathrm{e}^{i\epsilon_c \frac{4\pi}{\lambda_o} \int_0^t U_r(\tau) d\tau}, \tag{6.34}$$

and calculating its discrete values for t_n $(n = 1, ..., N)$ in Eq. (4.19).

Based on this synthetic radar signal time series, Fig. 3 shows results for the current estimation made with the MLE and the DM in a reasearch interval $[0 - 80]$ cm/s, every $\Delta t = 33$ s, by taking sliding intervals of $N = 512$ points ($T = 133$ s). Two levels of noise are tested for, $\sigma_{\mathcal{N}} = 0.1$ (low noise level) or $\sigma_{\mathcal{N}} = 1.5$ (high noise level), whose results are shown in Figs. 3a,b, respectively. Results show that the two methods perform equally well for the low noise level

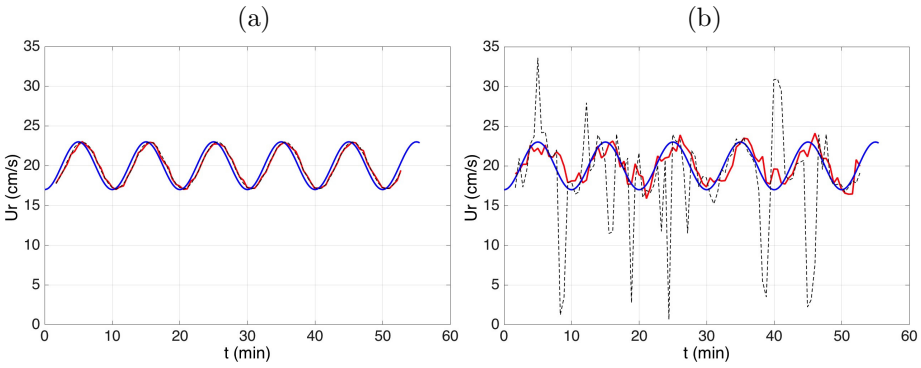

Figure 3: Time series of radial current magnitude estimated with: MLE (red lines), and DM (black dashed lines); from synthetic HF radar data with: (a) low, and (b) high noise levels. Sliding intervals of $N = 512$ points ($T = 133$ s) are used in the estimation, every 33 sec. The actual current from Eq. (6.33) is superimposed as blue lines.

(in fact there are little measurable differences between both), but for the high noise level, the DM exhibits erratic variations while the MLE keeps following the main trend of the actual oscillating current. Hence, in this first test case, even for very noisy data, the MLE is able to provide a fairly reliable estimate of a slowly varying current.

6.2. Robustness to wide-band signals

Here, we assess the robustness of the MLE approach for cases where the backscattered radar signal is perturbed by another deterministic broad band source. Let us assume for illustration that the available frequency band ($[-2, +2]$ Hertz at a 0.26 s sampling rate) is entirely contaminated by a chirp originating from another radio source, so that the backscattered signal (4.19) includes an additional "noise" of the form $n(t) = n_0 \exp\{2\mathrm{i}\pi(-2\mathrm{t} + 2\mathrm{t}^2/\mathrm{T})\}$, over an integration time T. Such a deterministic signal strongly deteriorates the Doppler spectrum, particularly regarding the identification of shifted Bragg lines (Fig. 4a). By contrast, the log-likelihood function computed with the MLE remains robust to this perturbation, showing a well-defined peak near the actual value of the radial surface current (Fig. 4b). In the example shown in Fig. 4, the signal was generated with $A^{\pm} = 1$, $\sigma_{\mathcal{N}} = n_0 = 5$, with a radial current value

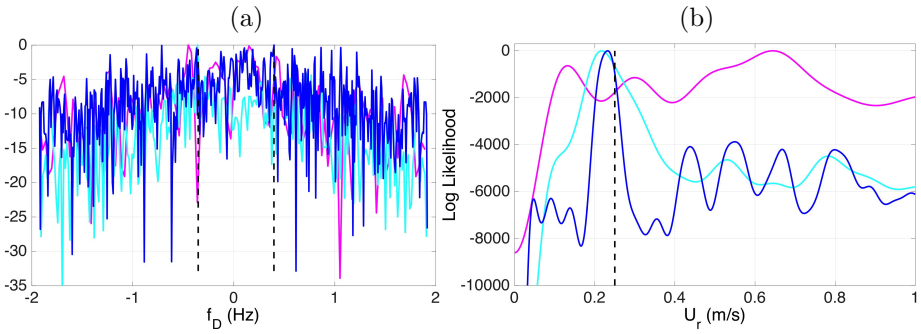

Figure 4: Doppler spectra (a) and Log-likelihood functions (b) obtained when the backscattered signal is contaminated by an external chirped source over the entire frequency band ($[-2, +2]$ Hertz) for different sample sizes N = (magenta) 128 ; (cyan) 256 and (blue) 512. The black dashed lines mark: (a) the position of the expected Bragg lines (including the shift caused by the current); (b) the actual value of the radial current $U_r = 0.25$ m/s.

$U_r = 25$ cm/s, and different sample sizes (N=128 or T=33 sec; N=256 or T=66 sec; N=512 or T=133 sec). The DM is unable to provide a relevant estimation of the radial current, while the MLE still provides an accurate estimation ($U_r = 0.217$ m/s with N=256 and 0.232 m/s with N=512).

7. Application to the Tofino WERA HF radar data

To mitigate the elevated tsunami hazard along the shores of Vancouver Island, BC (Canada), Ocean Networks Canada (ONC) has been developing a Tsunami Early Warning System combining instruments deployed on the seafloor, as part of their Neptune Observatory, and a shore-based WERA HF radar installed near Tofino (BC) (operational since April 2016). This radar has a carrier frequency $f_0 = 13.5$ MHz and can detect and estimate ocean radial currents up to a 85-110 km range, depending on sea state as propagation losses increase with sea surface roughness. The radar sweep area is outlined in Fig. 5 and is covered by a grid of radar cells, within which the received radar signal is averaged. There are 70 available cells in the range direction, with a radial step $\Delta R = 1.5$ km, for 121 sectors in the azimuthal direction, with angular opening $\Delta\phi_r = 1$ deg. The detection sector of the sweep area is 120 deg, implying that cells are

1.48 km wide at a 85 km range and narrower closer to the radar (cell area: $\Delta\mathbb{S} = R\,\Delta R\,\Delta\phi_r$ increases with range). The orientation of the radar array of 12 antennas (275 deg. from N, clockwise; centered at 49° 4' 24.82" N, 125° 46' 11.55" W) is such that one side of the sweep area boundary is nearly parallel to the coastline southeast of Tofino, and the array length (110 m) allows for an approximately 12 degree azimuthal resolution in the center of the sweep area, with a coarser resolution of about 20 degree near the edges of the scanned sector. In the beam forming algorithm, since the radar signal is processed for overlapping angular windows, surface currents can be estimated in a larger number of radar cells, with a 1 deg step size in azimuth. The different azimuths will be referred to by their number starting from the East.

We obtained a large amount of raw radar signal recorded by the Tofino HF radar system, at a sampling rate $\Delta t = 0.26$ s, and processed it in range and azimuth using software provided by Helzel Messtechnik GmbH (the radar vendor), to produce time series of complex backscattered signal $s(t)$ within each radar cell. No further processing was applied to the raw signal, in contrast with algorithms implemented in the WERA radar system, which is based on the spectral approach and applies a RFI elimination scheme in the spectrum computations. Within the available data set, a few complete days of records (referred to by their day number in year 2016) were processed, that represented different oceanic conditions; only a few generic examples are presented here. The basic recording format for the WERA coherent radar time series is the so-called "usort" file, which consists of a $T = 33$ sec duration sequence of $N = 128$ points at the said sampling rate. An example of 2 usort sequences (real and imaginary parts) is shown in Fig. 6. In the following examples, as in the previous section, we therefore consider integer multiples of these building blocks, by concatenating successive usort files (that is $N = 128$, 256, 512 points, etc).

Figure 6 shows examples of directly fitting the approximate backscattering model of Eq. (3.9) to radar signal time series $s(t)$ acquired at different ranges for short duration samples ($T = 66$ s). While a nearly perfect match is obtained at short range (gate 7; 10.5 km), the quality of the fit drastically deteriorates

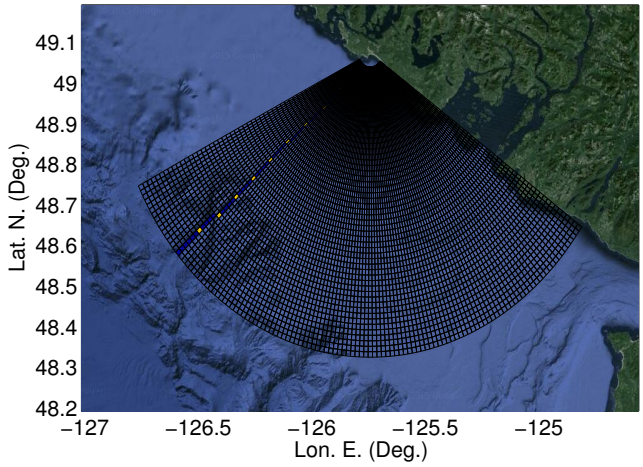

Figure 5: Grid of radar cells covering the Tofino, BC, WERA HF radar sweep area. The marked ray corresponds to azimuth 100 (40 degrees from boresight).

as range, and hence noise, increases (e.g., range 27; 40.5 km). As we shall see, an accurate estimation of the current based on the signal amplitude modulation, which is still visible at large range, remains possible with the MAPPE method, even though the instantaneous variations of the signal are no longer well represented.

The ability of the MLE and MAPPE methods to perform spatial current mapping over the entire Tofino HF radar sweep area is assessed next, and results are compared to those obtained with the DM of the optimized WERA radar system algorithms. For current spatial mapping using the MAPPE method, *a priori* information can be introduced in at least two ways: (i) using a long-time series, say 20 min, of radial currents evaluated in the recent past as a starting point for the updated estimation based on shorter time series; (ii) evaluating radial currents at increasing ranges and using results of a prior range n as input for the estimation at range $n + 1$. We tested the latter method for several days of radar data representing different oceanic conditions, and found results to be similar for the different days. Hence, in the following, we only present one day

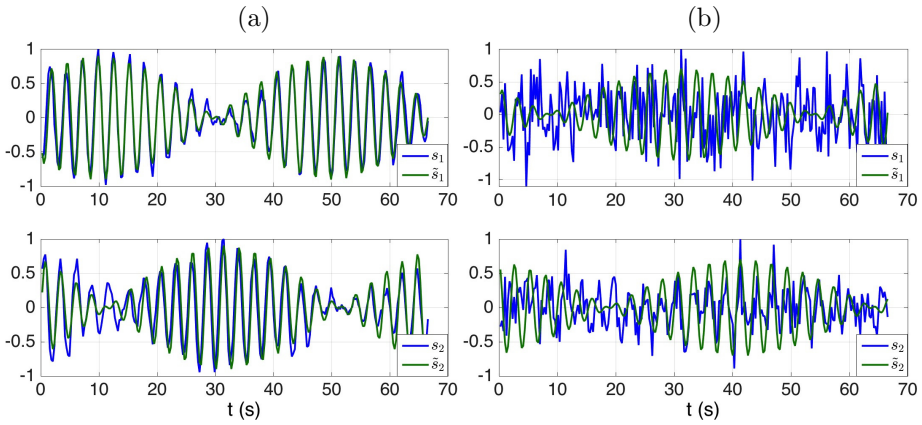

Figure 6: Data and reconstruction (tilde) with approximate Eq. (3.9) of the real and imaginary parts of the backscattered radar signal measured by the Tofino WERA HF radar on August 25th, 2016, for $T = 66$ s time series (2 usort files; $N = 256$ points) acquired at range: (a) 7 (10.5 km); (b) 27 (40.5 km).

of data, which can be considered as generic.

Figure 7 shows maps of the radial current over the Tofino WERA radar sweep area, inverted from data acquired on October 19th, 2016 (around 01.15 UTC). According to records made at the nearby NOAA buoy 46087[1], this was a day with low wind speed (3 m/s), but strong swell (2.36 m wave height and 12.9 s dominant wave period). These maps were calculated for two different sample sizes: $T = 33$ s, $N = 128$ points (Figs. 7a,b) and $T = 133$ s, $N = 512$ points (Figs. 7c,d). Figs. 7a,c show currents estimated with the MLE method while Figs. 7b,d show currents estimated with the MAPPE method. Fig. 7e, shows currents estimated with by the WERA system optimized software, based on the DM, and using the same 133 s sampling time. For MAPPE, values of the radial current were estimated by increasing both range and azimuth, using a prior normal distribution. Thus, the estimation at range n and azimuths $(m-1, m, m+1)$ was used as the central value for the prior distribution when estimating the current at range $n+1$ and azimuth m, with an assumed standard

[1] $http://www.ndbc.noaa.gov/station\_history.php?station = 46087$

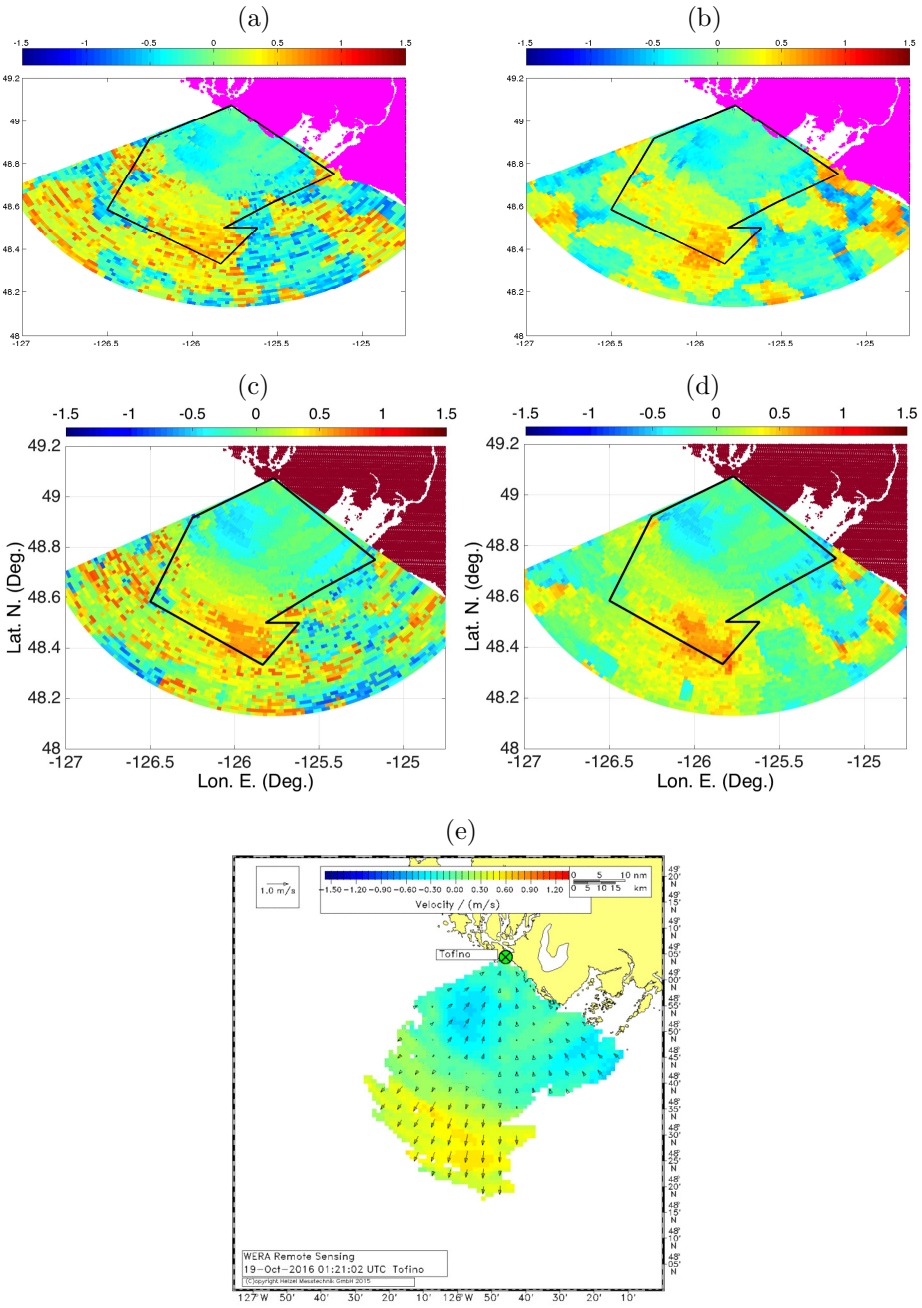

Figure 7: Maps of radial surface current U_r (color scale; m/s) inverted from Tofino WERA HF radar data acquired on Oct. 19th, 2016 (around 01:15 UTC), over the sweep area of Fig. 5, estimated with the: (a) MLE, 1 sample of $T = 33$ s ($N = 128$ points); (b) MAPPE, same sample; (c) MLE, 1 sample of $T = 133$ s ($N = 512$ points); (d) MAPPE, same sample; (e) optimized WERA's system software based on DM, using 1 sample of $T = 133$ s ($N = 512$ points) (courtesy of Helzel Messtechnick GmbH). Black lines in (a,b,c,d) approximately outline the area of available data in (e).

deviation $\sigma_{U_r} = 0.1$ m/s (dispersion parameter). The choice of the latter parameter was driven by physical considerations on how much the time-averaged current (here, over 2 min) can be allowed to vary between two neighboring cells. To further reduce errors on estimated values, a moving average was applied, over 3 cells in range and azimuth, to the signed (i.e., not the absolute value) of the estimated current.

Fig. 7 shows that, at short ranges, results of the MLE and MAPPE methods are consistent with each other, and also with WERA's system software results. Using a short sample duration $T = 33$ s already yields a good current estimation with both the MLE and MAPPE methods. At far ranges, however, the MLE method yields unrealistic noisy patterns of radial currents, likely due to the frequent occurrence of outliers in the estimation. Obvious current sign errors can be seen in the rapidly alternating and very contrasted red/blue areas in the farther ranges. By contrast, the MAPPE method yields a much cleaner and more realistic current pattern, with still some obvious sign errors near the furthermost corners of the radar sweep area. Such sign errors are possibly related to i) the increased antenna side lobes near these corners and the related increased currents variability; ii) a smaller SNR in these far ranges, which increases the dispersion in the estimation; iii) RFIs, which introduce spurious positive/negative Doppler frequencies . Since, unlike in the standard WERA system software, we did not perform any specific treatment to reduce noise and eliminate RFIs, we believe that there is great room for improvement of the probabilistic method by implementing similar techniques of RFI reduction as those used with the DM approach. This will be tested in future work.

8. A critical discussion

Based on the above results, we briefly discuss below some features of the proposed method, including issues and limitations. Any of these might warrant a more in-depth study, but these developments will be left out for forthcoming work and papers.

8.1. Accuracy

An important concept in the framework of estimation is accuracy. In the classical Doppler-based (DM) estimation, the accuracy of estimated currents is characterized by the width of the first-order Bragg peak. With a probabilistic method, however, assessing the accuracy of current estimates is far less obvious and it is important to first properly define it. What would make sense with the proposed method is establishing a confidence interval (CI) of the estimated value, that is a given interval around it, with a certain high quantile of the distribution (for example, a 95% CI). However, in the present context, accuracy very much depends on noise level, as seen for instance in Fig. 2, which shows the evolution of the rms error (standard deviation) of the estimated radial current with noise level. Note, even with the DM, the theoretical accuracy of the estimation based on the Bragg peak centroïd only holds in the noise free case, while the actual resolution deteriorates with increasing noise, as can be seen for instance in Fig. 4. However, one point is clear from our results, namely that, similar to the DM, the accuracy of the probabilistic method increases with sample size (as long as the latter remains smaller than the temporal scale of ocean variability). This is illustrated in Fig. 8a, which shows an example of MLE log-likelihood function computed for a noise-free signal based on the first-order Bragg model Eq. (4.19), with $U_c = 0.25$ m/s. Here, the main peak of the distribution becomes sharper and more pronounced as the number of samples N is increased from 64 to 1,024. Besides N, other parameters affect the accuracy, namely the noise level σ_N (here taken to be 3 times the signal amplitude in Eq. 4.19), which can widen and displace the main peak of the distribution, particularly for small N values (Fig. 8b), and the Bragg amplitude ratio ρ (the peak of the distribution being far less contrasted in the case of a single Bragg amplitude; see dashed lines in Figs. 8a,b). To summarize, the accuracy of the MLE method can only be rigorously defined as a CI, with respect to some quantile, which depends on integration time T (or sample size N), noise level σ_N, and Bragg amplitude ratio ρ. Such a CI can only be derived through a statistical analysis, by performing Monte Carlo simulations over many samples covering the

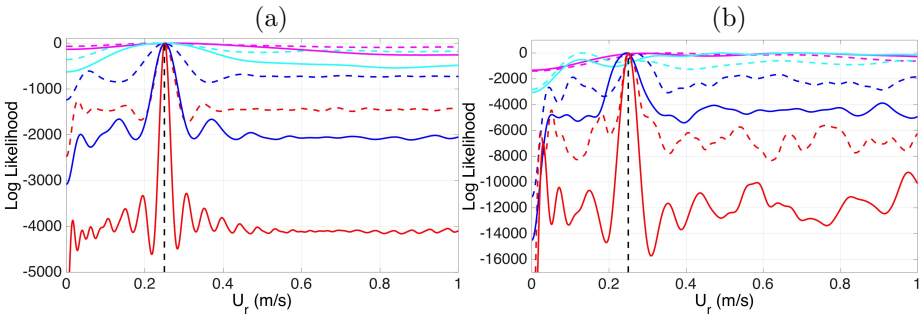

Figure 8: MLE log-likelihood function as a function of trial radial current, for a signal simulated with first-order Bragg model Eq. (4.19): (a) without; and (b) with, noise. The colored lines correspond to different sample sizes N = (magenta) 64; (cyan) 128; (blue) 512; and (red) 1024, with solid lines corresponding to a Bragg ratio $\rho = 1$ and dashed lines to a $\rho = 0$. Black vertical dashed lines mark the location of the actual current value (0.25 m/s). The maximum log-likelihood values have been normalized to zero.

range of parameter values; hence, there is no a priori simple estimation of the method accuracy. Assessing such accuracy can thus only be achieved through a comparison with other instrument measurements and any kind of sea-truthing.

8.2. Current sign

A weakness of the MLE method is the more frequent occurrence of sign errors in the radial surface current estimates, as the noise level increases. This is illustrated by the spotty aspect of the maps of Fig. 7 in the far-ranges and can partly be compensated by averaging the sign other several cells, to prevent from unrealistic sign changes from one cell to another. Hence, when estimating the current in the far-ranges, it is useful to complement the map of algebraic radial current by a map of the absolute value of radial currents, which is more robust to noise. This shortcoming of the method is one point to be addressed in future work and we have some hope that this can be improved upon by applying an adequate RFI processing.

8.3. Second-order spectrum

The MLE method is solely based on first-order Bragg theory, with second-order effects being ignored. It is well known that such effects may become

important for higher frequency radars, and in higher sea states (i.e., steeper waves). In the Doppler spectrum, second-order effects can produce swell peaks, which in some cases can be very close to, and thus contaminate, the main Bragg lines. They can also broaden the first-order peaks if the Doppler resolution is insufficient. Hence, second-order effects can be an additional source of error in the model and thus deserve a specific study, which is left out for further work. In the meantime, our preliminary numerical tests, based on numerical simulations, indicate that the MLE method is robust to the presence of swell peaks.

8.4. CPU time

The estimation of the radial surface currents with the DM is numerically efficient, as it is based on FFTs which require an $O(N\log(N))$ CPU time, where N is the time series length. The probabilistic MLE method requires the evaluation of a cost function for every trial current and therefore has a computational cost in $O(N \times N_c)$, where N_c is the number of trial values used for the surface current estimation. The CPU time of the new method, hence, strongly depends on the latter, which is related to the accuracy of the estimation, since increasing N_c allows better resolving the main peak of the log-likelihood function. However, our experience is that N_c can be kept fairly low in practice, so that computational time with the MLE remains small, even though it is found slightly larger than for the DM (although it only takes a few seconds to generate an entire current map on a laptop). Moreover, a good a priori knowledge of the surface current search interval helps dramatically reduce the required number of trial values and thus greatly accelerate the estimation.

8.5. Radar types

As already mentioned, this non-spectral method requires that the range-azimuth resolved radar signal be available in the time domain. This precludes using data from compact radar systems, where the azimuthal discrimination is performed in the frequency domain via a direction finding algorithm.

9. Conclusions

We presented a new probabilistic method to process HF radar data for estimating oceanic radial surface currents, which provides an alternative to the Doppler-based method that has been in use for more than four decades. This new method is based on identifying an amplitude modulation of the Bragg frequency in the real and imaginary parts of the complex backscattered radar signal. The absolute radial current, which is responsible for this modulation, is found using a Maximum Likelihood approach, for a simplified radar signal model based on first-order Bragg theory. A refined estimation can be obtained with a Bayesian analysis, which uses an *a posterior* probability distribution of the absolute radial current, based on a reasonable *prior distribution*, with parameters estimated from earlier current observations or physical assumptions on its range and variability in the considered region. Our investigations so far have shown that this probabilistic approach can be a useful complementary method for estimating the radial surface currents, particularly in cases of weak SNR or for a rapid temporal variability of the current, requiring shorter observation times to be captured. Some limitations of the method have been identified, such as errors occurring in the estimation of the radial current sign in the most distant ranges and biased estimates for small current values. However, we believe that this new approach has a promising range of potential applications and thus deserves further validation, particularly on the basis of independently measured surface currents. This will be the object of future work.

Acknowledgments. The authors gratefully acknowledge Helzel Messtechnik GmbH, in particular Dr. A. Dzvonkovskaya, for technical support and software to process the radar data in range and azimuth, and T. Helzel for useful comments and advices on the manuscript. Ocean Network Canada is acknowledged for providing data from their Tofino WERA radar and support to the University of Rhode Island (URI) to conduct this research. C.-A. Guérin also acknowledges the CNRS, the University of Toulon, and the French-American Fulbright commission, for supporting his stay at URI over 2016-2017.

10. Appendix

In the following, we derive the approximate Eq. (3.9) of the radar signal. Starting from Eq. (3.6) and using some elementary trigonometric relationships, we can recast s_1 and s_2 in the form,

$$\begin{aligned} s_1(t) &= \alpha^+ \cos(\omega_B t)\cos(\omega_c t - \psi^+) + \alpha^- \sin(\omega_B t)\cos(\omega_c t - \psi^-) \\ s_2(t) &= \alpha^+ \cos(\omega_B t)\sin(\omega_c t - \psi^+) + \alpha^- \sin(\omega_B t)\sin(\omega_c t - \psi^-), \end{aligned} \tag{10.35}$$

with,

$$\begin{aligned} \alpha^\pm &= \sqrt{(A^-)^2 + (A^+)^2 \pm 2A^-A^+\cos(\varphi^+ - \varphi^-)} \\ \tan\psi^+ &= \frac{A^-\sin\varphi^- + A^+\sin\varphi^+}{A^-\cos\varphi^- + A^+\cos\varphi^+} \\ \tan\psi^- &= \frac{-A^-\cos\varphi^- + A^+\cos\varphi^+}{A^-\sin\varphi^- - A^+\sin\varphi^+} \end{aligned} \tag{10.36}$$

If the time series is long enough it is always possible to find some $t_1^\pm$ and $t_2^\pm$ values such that,

$$\begin{aligned} \omega_B t_1^+ &= \omega_B t_2^+ = 0 \bmod 2\pi \\ \omega_B t_1^- &= \omega_B t_2^- = \pi/2 \bmod 2\pi \\ \omega_c t_1^\pm &= \psi^\pm \bmod 2\pi \\ \omega_c t_2^\pm &= \psi^\pm + \pi/2 \bmod 2\pi \end{aligned} \tag{10.37}$$

and therefore rewrite Eq. (10.35) as,

$$\begin{aligned} s_1(t) &= \alpha^+ \cos(\omega_B(t - t_1^+)))\cos(\omega_c(t - t_1^+)) + \alpha^- \cos(\omega_B(t - t_1^-))\cos(\omega_c(t - t_1^-))) \\ s_2(t) &= \alpha^+ \cos(\omega_B(t - t_2^+))\cos(\omega_c(t - t_2^+)) + \alpha^- \cos(\omega_B(t - t_2^-))\cos(\omega_c(t - t_2^-)), \end{aligned} \tag{10.38}$$

Eq. (3.9) is exactly recovered whenever $\alpha^- = 0$ or $\alpha^+ = 0$; otherwise, it is only an approximation that can be used with,

$$\alpha \simeq \max(\alpha^-, \alpha^+) = \sqrt{(A^-)^2 + (A^+)^2 + 2A^-A^+\left|\cos(\varphi^+ - \varphi^-)\right|} \tag{10.39}$$

and $(t_1, t_2) = (t_1^+, t_2^+)$ if $\alpha = \alpha^+$ or $(t_1, t_2) = (t_1^-, t_2^-)$ if $\alpha = \alpha^-$. For this approximate parametric identification to hold, one needs to verify that

$\max(s_1) \simeq \max(s_2) \simeq \max(\alpha^-, \alpha^+)$ and that $(t_1^\pm, t_2^\pm)$ are the actual times of the maxima of (s_1, s_2). This has been numerically assessed by verifying that,

$$\Delta\alpha = 1 - \frac{\max(\alpha^-, \alpha^+)}{\max(s_1)}, \tag{10.40}$$

computed as a function of $\varphi = \varphi^+ - \varphi^-$ and $\rho = \min(A^-, A^+)/\max(A^-, A^+)$ is small, and that the product,

$$P = \cos(\omega_B t_1)\cos(\omega_c t - \psi^+) \text{ or } P = \sin(\omega_B t_1)\cos(\omega_c t - \psi^-), \tag{10.41}$$

depending on whether, $\alpha = \alpha^+$ or $\alpha = \alpha^-$, is close to 1.

References

[1] D. E. Barrick, HF radio oceanography a review, Boundary-Layer Meteorology 13 (1-4) (1978) 23–43.

[2] D. Prandle, A new view of near-shore dynamics based on observations from HF radar, Progress in oceanography 27 (3-4) (1991) 403–438.

[3] J. D. Paduan, L. Washburn, High-frequency radar observations of ocean surface currents, Annual review of marine science 5 (2013) 115–136.

[4] L. R. Wyatt, et al., HF radar: Applications in coastal monitoring, planning and engineering, in: Coasts and Ports 2013: 21st Australasian Coastal and Ocean Engineering Conference and the 14th Australasian Port and Harbour Conference, Engineers Australia, 2013, p. 878.

[5] M. Heron, R. Gomez, B. Weber, A. Dzvonkovskaya, T. Helzel, N. Thomas, L. Wyatt, Application of HF radar in hazard management, International Journal of Antennas and Propagation 2016.

[6] B. J. Lipa, D. E. Barrick, J. Bourg, B. B. Nyden, HF radar detection of tsunamis, Journal of Oceanography 62 (5) (2006) 705–716.

[7] K.-W. Gurgel, A. Dzvonkovskaya, T. Pohlmann, T. Schlick, E. Gill, Simulation and detection of tsunami signatures in ocean surface currents measured by HF radar, Ocean Dynamics 61 (10) (2011) 1495–1507.

[8] D. B. B Lipa, J. Isaacson, Tsunami, Environmental Sciences, InTech, 2016, Ch. Chapter 5: Coastal Tsunami Coastal Tsunami Warning with Deployed HF Radar Systems, pp. 73–112.

[9] S. T. Grilli, C. A. Guérin, M. Shelby, A. R. Grilli, P. Moran, S. Grosdidier, T. L. Insua, Tsunami detection by High Frequency Radar beyond the continental shelf: II. Extension of algorithms and validation on realistic case studies, Pure and Appl. Geophys. 174 (1) (2017) 3003–3028. doi:10.1007/s00024-017-1619-6.

[10] M. Berta, L. Bellomo, M. G. Magaldi, A. Griffa, A. Molcard, J. Marmain, M. Borghini, V. Taillandier, Estimating lagrangian transport blending drifters with HF radar data and models: results from the TOSCA experiment in the ligurian current (north western mediterranean sea), Progress in Oceanography 128 (2014) 15–29.

[11] J. Helbig, P. Pepin, The effects of short space and time scale current variability on the predictability of passive ichthyoplankton distributions: an analysis based on HF radar observations, Fisheries Oceanography 11 (3) (2002) 175–188.

[12] A. Parks, L. K. Shay, W. E. Johns, J. Martinez-Pedraja, K.-W. Gurgel, HF radar observations of small-scale surface current variability in the straits of florida, Journal of Geophysical Research: Oceans 114 (C8).

[13] A. C. Haza, T. M. Özgökmen, A. Griffa, A. Molcard, P.-M. Poulain, G. Peggion, Transport properties in small-scale coastal flows: relative dispersion from VHF radar measurements in the gulf of la spezia, Ocean Dynamics 60 (4) (2010) 861–882.

[14] S. Webb, X. Zhang, W. Crawford, Infragravity waves in the deep ocean, Journal of Geophysical Research 96 (C2) (1991) 2723–2736.

[15] D. D. Crombie, Doppler spectrum of sea echo at 13.56 mc./s., Nature 175 (4459) (1955) 681–682.

[16] D. E. Barrick, First-order theory and analysis of MF/HF/VHF scatter from the sea, Antennas and Propagation, IEEE Transactions on 20 (1) (1972) 2–10.

[17] D. E. Barrick, Remote sensing of sea state by radar, in: Engineering in the Ocean Environment, Ocean 72-IEEE International Conference on, IEEE, 1972, pp. 186–192.

[18] D. E. Barrick, Remote sensing of the troposphere, Remote Sensing of Sea State by Radar (1972) 1–46.

[19] D. E. Barrick, Remote sensing of sea state by radar, remote sensing of the troposphere, ve derr, editor, us govt, Printing Office, Washington, DC 12.

[20] R. H. Stewart, J. W. Joy, HF radio measurements of surface currents, in: Deep Sea Research and Oceanographic Abstracts, Vol. 21, Elsevier, 1974, pp. 1039–1049.

[21] K.-W. Gurgel, H.-H. Essen, S. Kingsley, High-frequency radars: physical limitations and recent developments, Coastal engineering 37 (3) (1999) 201–218.

[22] D. Barrick, Accuracy of parameter extraction from sample-averaged sea-echo doppler spectra, IEEE Transactions on Antennas and Propagation 28 (1) (1980) 1–11.

[23] P. Forget, Noise properties of HF radar measurement of ocean surface currents, Radio Science 50 (8) (2015) 764–777.

[24] K.-W. Gurgel, Y. Barbin, T. Schlick, Radio frequency interference suppression techniques in FMCW modulated HF radars, in: OCEANS 2007-Europe, IEEE, 2007, pp. 1–4.

[25] K.-W. Gurgel, T. Schlick, Remarks on signal processing in HF radars using FMCW modulation, in: Proc. IRS, 2009, pp. 1–5.

[26] T. Helzel, M. Kniephoff, Software beam forming for ocean radar WERA features and accuracy, in: OCEANS 2010, IEEE, 2010, pp. 1–3.

[27] L. R. Wyatt, J. J. Green, A. Middleditch, Signal sampling impacts on HF radar wave measurement, Journal of Atmospheric and Oceanic Technology 26 (4) (2009) 793–805.

[28] L. R. Wyatt, J. B. Jaffrés, M. L. Heron, Spatial averaging of HF radar data for wave measurement applications, Journal of Atmospheric and Oceanic Technology 30 (9) (2013) 2216–2224.

[29] P. Stoica, R. L. Moses, et al., Spectral analysis of signals, Vol. 452, Pearson Prentice Hall Upper Saddle River, NJ, 2005.

[30] R. H. Khan, Ocean-clutter model for high-frequency radar, IEEE Journal of Oceanic Engineering 16 (2) (1991) 181–188.

[31] R. Martin, M. Kearney, Remote sea current sensing using hf radar: An autoregressive approach, IEEE journal of oceanic engineering 22 (1) (1997) 151–155.

[32] A. Middleditch, L. Wyatt, An instantaneous-frequency filtering technique for high-frequency radar oceanography, IEEE Journal of Oceanic Engineering 31 (4) (2006) 797–803.